# Local and Average Structures and Magnetic Properties of $Sr_2FeMnO_{5+y}$, $y$ = 0.0, 0.5. Comparisons with $Ca_2FeMnO_5$ and the Effect of the A-Site Cation

Farshid Ramezanipour,[†,‡] John E. Greedan,*[,†,‡] Joan Siewenie,[§] Th. Proffen,[§] Dominic H. Ryan,[||] Andrew P. Grosvenor,[⊥] and Ronald L. Donaberger[#]

[†]Department of Chemistry and [‡]Brockhouse Institute for Materials Research, McMaster University, 1280 Main Street West, Hamilton, Ontario L8S 4M, Canada

[§]Lujan Neutron Scattering Center, Los Alamos National Laboratory, Los Alamos, New Mexico 87545, United States

[||]Physics Department and Centre for the Physics of Materials, McGill University, 3600 University Street, Montreal, Quebec H3A 2T8, Canada

[⊥]Department of Chemistry, University of Saskatchewan, Saskatoon, Saskatchewan S7N 5C9, Canada

[#]Canadian Neutron Beam Centre, Chalk River, Ontario K0J 1J0, Canada

**ABSTRACT:** $Sr_2FeMnO_{5+y}$ was synthesized under two different conditions, in air and in argon, both of which resulted in a cubic, $Pm\bar{3}m$, structure with no long-range ordering of oxygen vacancies. The unit cell constants were found to be $a_0$ = 3.89328(1) Å for argon ($y$ = 0.0) and $a_0$ = 3.83075(3) Å for air ($y$ = 0.5). In contrast, $Ca_2FeMnO_5$ retains long-range brownmillerite oxygen vacancy ordering for either air or argon synthesis. Remarkably, $Sr_2FeMnO_{5.0}$ oxidizes spontaneously in air at room temperature. A neutron pair distribution function (NPDF) study of $Sr_2FeMnO_{5.0}$(Ar) showed evidence for local, brownmillerite-like ordering of oxygen vacancies for short distances up to 5 Å. Mössbauer spectroscopy results indicate more than one Fe site for $Sr_2FeMnO_{5+y}$(Ar and air), consistent with the noncubic local structure found by NPDF analysis. The isomer



shifts and quadrupole splittings in both air- and argon-synthesized materials are consistent with the 3+ oxidation state for Fe in sites with coordination number four or five. This is confirmed by an L-edge XANES study. Mn is almost entirely in the 3+ state for $Sr_2FeMnO_{5.0}$(Ar), whereas $Mn^{4+}$ is predominantly present for $Sr_2FeMnO_{5.5}$(air). Magnetic susceptibility data show zero-field-cooled/field-cooled (ZFC/FC) divergences near 50 K for the Ar sample and 25 K for the air sample, whereas $Ca_2FeMnO_5$ is long-range G-type antiferromagnetically ordered at 407(2) K. Hyperfine magnetic splitting, observed in temperature-dependent Mössbauer measurements, indicates short-range magnetic correlations that persist up to 150 K for $Sr_2FeMnO_{5.0}$(Ar) and 100 K for $Sr_2FeMnO_{5.5}$(air), well above the ZFC/FC divergence temperatures. Neutron diffraction data confirm the absence of long-range magnetic ordering at room temperature and 4 K for $Sr_2FeMnO_{5.0}$(Ar) but indicate the presence of domains with short-range G-type order at 4 K with an average dimension of ~50 Å ($y$ = 0); thus, this material is actually a superparamagnet rather than a true spin glass. In sharp contrast, corresponding data for $Sr_2FeMnO_{5.5}$(air) show mainly a very weak magnetic Bragg peak, indicating that ~4% of the sample has G-type antiferromagnetic ordering at 4 K.
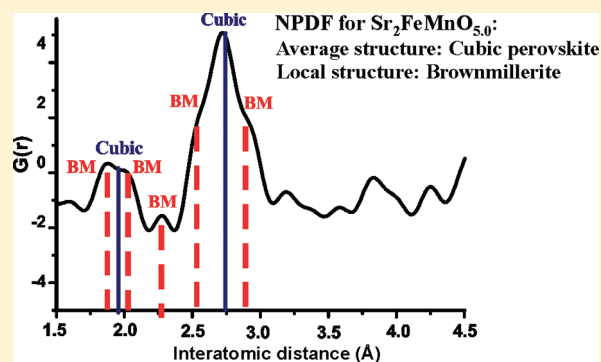
## ■ INTRODUCTION

Oxygen-deficient perovskites can have a variety of structures depending on different factors including the degree of anion deficiency and the composition. In this article, the focus is on oxygen-deficient perovskites with the formula $A_2BB'O_{5+x}$. The oxygen vacancies can order to form the brownmillerite structure in which the B cations are octahedrally coordinated, forming corner-sharing layers, and the B′ cations are tetrahedrally coordinated, forming corner-sharing chains. (Figure 1). This long-range vacancy ordering results in a supercell that generally has dimensions with respect to the cubic perovskite cell constant, $a_p$,

of $a_{br} \approx 2^{1/2}a_p$, $b_{br} \approx 4a_p$, and $c_{br} \approx 2^{1/2}a_p$. A number of different space group symmetries are observed, depending on subtle differences in the ordering of the tetrahedral chains within the unit cell. The chains can show either a right-handed (R) or left-handed (L) orientation and the correlation between the intra- and interlayer chain orientations and the resulting space groups are summarized in Table 1. As shown in this table, if all chains have the same orientation in all layers, the space group will be
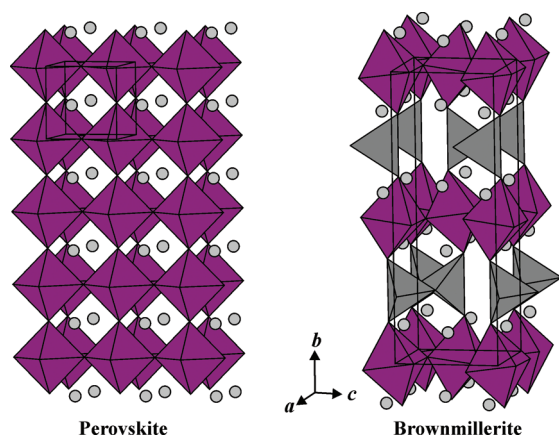
**Figure 1.** Comparison between the disordered perovskite and brownmillerite structures. The disordered perovskite structure consists of a network of corner-sharing octahedra with oxygen vacancies randomly occupying the corner sites (left), whereas in brownmillerite (right), the oxygen vacancies order to form layers of octahedra separated by chains of tetrahedra. The resulting brownmillerite superstructure is described by a unit cell of dimensions $a_{br} \approx 2^{1/2} a_p$, $b_{br} \approx 4a_p$, and $c_{br} \approx 2^{1/2} a_p$, but a number of space group symmetries are observed. (See text.)

*I2mb*. The same chain orientation within each layer but opposite in the adjacent layer results in space group *Pnma*. Alternating R and L orientations within each layer and between the layers gives rise to space groups *Pcmb* and *C2/c*. Finally, if the ordering of chains is absent, the space group will be *Imma*. Although many oxygen-deficient perovskites of composition $A_2BB'O_{5+x}$ adopt the brownmillerite structure, there are exceptions, noted below, especially when Jahn–Teller ions such as $Mn^{3+}$ are involved.

Oxygen-deficient perovskites containing Fe and Mn as B/B' site ions and Ca and Sr as A-site cations have previously been reported. The iron-containing brownmillerite compounds $Ca_2Fe_2O_5$ and $Sr_2Fe_2O_5$ have been synthesized and studied.[1−3] These two materials exhibit one example of the effect of the A-site cation on the structure; $Ca_2Fe_2O_5$ crystallizes in the *Pnma* space group,[1] whereas $Sr_2Fe_2O_5$ belongs to the *Icmm* (*Imma*) space group.[2,3] The role of the larger Sr cation here is to disorder the chain orientations with respect to the Ca-based compound.

Both of these materials show long-range antiferromagnetic (AF) ordering with $T_c > 700$ K.[4−7] In addition, materials with the formula $Sr_2Fe_2O_{5+x}$, $0 < x < 1$,[8,9] show further oxide vacancy ordering and crystallize in the *Cmmm* ($x = 0.5$) and *I4/mmm* ($x = 0.75$) space groups.[9] A highly oxidized, disordered structure, $Pm\overline{3}m$, with $x \approx 1$, can also be obtained by firing the sample in pure oxygen.[9] However, the oxidized samples can be reduced to $Sr_2Fe_2O_5$ by annealing in inert gas.[10]

Now, with Mn on the B/B' sites, both $Ca_2Mn_2O_5$ and $Sr_2Mn_2O_5$ have been synthesized. These materials do not adopt the brownmillerite structure, but instead, the B-site cations occupy a unique site with square-pyramidal geometry.[11−13] Although both of these materials are orthorhombic, the effect of the A-site cation can again be seen in the space group symmetry. $Ca_2Mn_2O_5$ crystallizes in space group *Pnma*, whereas for $Sr_2Mn_2O_5$, the space group is *Pbam*. It is noteworthy that, in the above cases, the change in A-site cation results in a change in space group, whereas the general structural type remains the same. Both $Ca_2Fe_2O_5$ and $Sr_2Fe_2O_5$ are brownmillerites and contain alternating layers of octahedra and tetrahedra. Also, in both $Ca_2Mn_2O_5$ and $Sr_2Mn_2O_5$, the geometry around all Mn sites is

**Table 1. Correlations between the Intra- and Interlayer Tetrahedral (T) Chain Orientations and the Resulting Space Groups for Brownmillerites**[a]

| ordering within one T-layer | ordering in the neighboring T-layer | space group |
|---|---|---|
| L—L—L | L—L—L | |
| R—R—R | R—R—R | *I2mb* |
| L—L—L | R—R—R | |
| R—R—R | L—L—L | *Pnma* |
| L—R—L | R—L—R | |
| R—L—R | L—R—L | *Pcmb, C2/c*[b] |
| none | none | *Imma* |

[a] L and R denote left- and right-handed chains, respectively. [b] For *Pbcm* and *C2/c*, $c_{br} \approx 2 \times 2^{1/2} a_p$, and there are two distinct tetrahedral sites per layer.

square-pyramidal. In this article, however, we show that the effect of the A-site cation is more significant when both Fe and Mn are present in the same $A_2BB'O_{5+x}$ compound. The synthesis, crystal structure, local structure, and magnetic properties of $Sr_2FeMnO_{5.0}$ and $SrFeMnO_{5.5}$, prepared in argon and air atmospheres, respectively, are described and compared with the previously studied material, $Ca_2FeMnO_5$.[14] $Sr_2FeMnO_{5+y}$ has been reported, prepared in an air atmosphere, to be cubic with a cell constant $a = 3.852$ Å, but no further details are available.[15]

## ■ EXPERIMENTAL SECTION

**Synthesis.** $Sr_2FeMnO_{5+y}$ and $Ca_2FeMnO_{5+y}$ were synthesized using stoichiometric amounts of $SrCO_3$ (99.9% Sigma Aldrich), $CaCO_3$ (99.9% Sigma Aldrich), $Fe_2O_3$ (99.998% Alfa Aesar), and $Mn_2O_3$ (99.9% Cerac) that were mixed and pressed into pellets. The pellets were annealed at 1250 °C in an argon atmosphere for a total time of ~100 h and were then slowly cooled to room temperature. Several intermediate grindings were performed. The heating and cooling rates were both 100 °C/h. The syntheses were also carried out in an air atmosphere using the same heating and cooling protocol to determine the effect of synthesis conditions on structure and physical properties.

**X-ray and Neutron Diffraction.** X-ray powder diffraction data were obtained using a PANalytical X'Pert Pro MPD diffractometer with a linear X'Celerator detector with CuKα₁ radiation ($\lambda = 1.54056$ Å) and a 2θ step interval of 0.0084° at room temperature.

Room-temperature time-of-flight neutron-scattering data were collected on the instrument NPDF at the M. J. Lujan Jr. Center for Neutron Scattering at the Los Alamos Neutron Science Center.[16] Constant-wavelength neutron data were obtained at the Canadian Neutron Beam Centre on the C2 diffractometer with wavelengths $\lambda = 1.33$ and 2.37 Å at room temperature and 4 K.

**Thermal Gravimetric Analysis (TGA).** TGA experiments were performed on a Netzsch STA-409 TGA—DTA (thermal gravimetric analyzer—differential thermal analyzer) instrument by heating the air-synthesized samples in argon at a rate of 5 °C/min, to 1225 °C, and measuring the weight losses.

**Magnetic Property Measurements.** Bulk magnetic measurements were performed using a Quantum Design MPMS SQUID magnetometer. The zero-field-cooled/field-cooled (ZFC/FC) magnetic susceptibility data, as well as isothermal magnetization data, were obtained on a powder sample in a gelatin capsule in the temperature
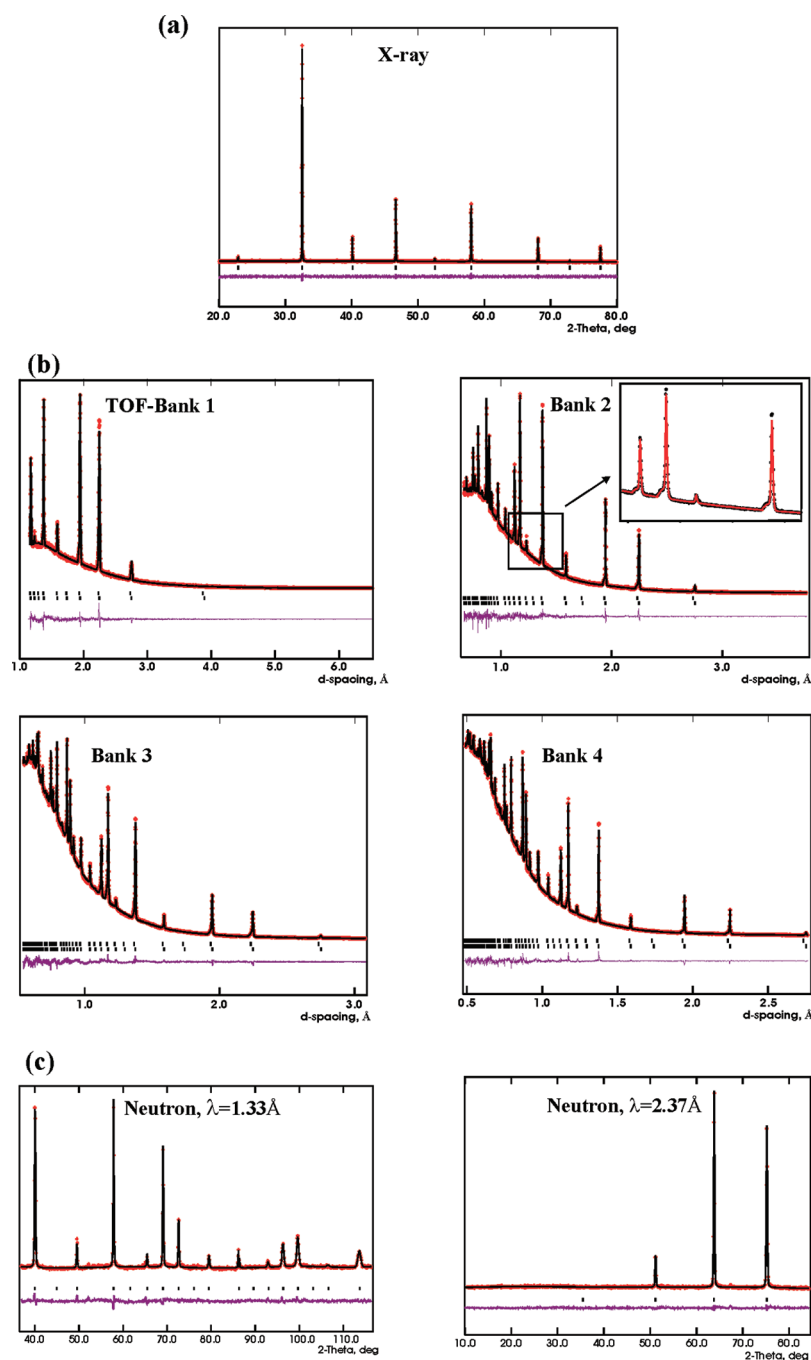
**Figure 2.** Rietveld refinement profiles for $Sr_2FeMnO_{5.0}(Ar)$ obtained from (a) powder X-ray diffraction data with $\lambda = 1.54056$ Å; (b) time-of-flight neutron diffraction data collected at detector angles of 46° (bank 1), 90° (bank 2), 119° (bank 3), and 148° (bank 4); and (c) constant-wavelength neutron with two different wavelengths. The stars are the experimental data, the solid line is the model, the vertical tic marks locate Bragg peak positions, and the lower line is the difference plot.

range of 5–300 K. A quartz sample holder was used for the susceptibility measurement from 320 to 700 K.

**Mössbauer Spectroscopy.** [57]Fe Mössbauer spectra were obtained in transmission mode on a conventional constant-acceleration spectrometer using a 50 mCi [57]CoRh source. The spectrometer was calibrated using α-Fe foil at room temperature, and all isomer shifts were measured relative to the centroid of the calibration spectrum. Temperatures down to 5 K were obtained using a vibration-isolated closed-cylcle fridge with the sample in helium exchange gas. Typical stabilities were better than 0.01 K during the measurements. The spectra were fitted

using a conventional nonlinear least-squares minimization routine to a sum of equal-width Lorentzian lineshapes. Several distinct models were used. The basic approach was to use a sum of paramagnetic quadrupole doublets or magnetic sextets with line positions determined from a first-order perturbation calculation; however, in some cases, a Gaussian distribution of quadrupole splittings with a correlated isomer shift distribution was employed, and some of the magnetic patterns were fitted using a model-free distribution of hyperfine fields based on Window's method.[17]

**X-ray Absorption Near-Edge Spectroscopy (XANES).** To determine the Fe and Mn oxidation states and local coordination

**Table 2. Refinement Results with X-ray (300 K), TOF (300 K), and Constant-Wavelength Neutron Diffraction Data (290 K) for $Sr_2FeMnO_{5.0}$ Synthesized in Argon Atmosphere**

| | |
|---|---|
| space group | $Pm\bar{3}m$ |
| lattice parameters | $a = 3.89328(1)$ Å |
| | $V = 59.0130(10)$ Å$^3$ |
| Z | 1 |
| agreement factors | $R_p$ (X-ray, $\lambda = 1.54056$ Å) = 0.0265 |
| | $R_{wp}$ (X-ray, $\lambda = 1.54056$ Å) = 0.0348 |
| | $R_p$ (TOF, four banks) = 0.0172 |
| | $R_{wp}$ (TOF, four banks) = 0.0263 |
| | $R_p$ (neutron, $\lambda = 1.32858$ Å) = 0.0370 |
| | $R_{wp}$ (neutron, $\lambda = 1.32858$ Å) = 0.0481 |
| | $R_p$ (neutron, $\lambda = 2.36950$ Å) = 0.0410 |
| | $R_{wp}$ (neutron, $\lambda = 2.36950$ Å) = 0.0538 |

**Table 3. Atomic Coordinates, Site Occupancies and Displacement Factors for $Sr_2FeMnO_{5.0}$(Ar) Obtained from Powder Neutron Diffraction Data**

| | $x$ | $y$ | $z$ | occupancy | $U_{iso}$ (Å$^2$) |
|---|---|---|---|---|---|
| | | | TOF, at 300 K | | |
| Sr | 0.5 | 0.5 | 0.5 | 1.0 | 0.0148(2) |
| Fe | 0 | 0 | 0 | 0.522(3) | 0.0340(7) |
| Mn | 0 | 0 | 0 | 0.478(3) | 0.0340(7) |
| O | 0.5 | 0 | 0 | 0.833(5) | 0.0283(2) |
| | | $\lambda = 1.32858$ and $\lambda = 2.36950$, at 290 K, simultaneous refinement | | | |
| Sr | 0.5 | 0.5 | 0.5 | 1.0 | 0.024(2) |
| Fe | 0 | 0 | 0 | 0.475(9) | 0.028(3) |
| Mn | 0 | 0 | 0 | 0.525(9) | 0.028(3) |
| O | 0.5 | 0 | 0 | 0.78(2) | 0.0311(8) |

environments in the materials investigated here, Fe and Mn L-edge XANES spectra were collected at the Canadian Light Source using the spherical grating monochromator (SGM) undulator beamline, 11ID-1.[18] The flux was $\sim 10^{11}$ photons/s at 1900 eV and increased to $\sim 4 \times 10^{12}$ photons/s at 250 eV. The resolution was better than 0.3 eV at photon energies below 1500 eV, and the instrumental precision was better than $\pm 0.1$ eV. Powdered samples were mounted on carbon tape and measured in vacuo. Total electron yield (TEY) and X-ray fluorescence yield (FLY) spectra were collected simultaneously. TEY spectra are presented for the Fe and Mn L-edges. Spectra were collected from $\sim 30$ eV below the absorption edge to $\sim 50$ eV above the edge to get a suitable background for normalization. All spectra were collected with a 0.1 eV step size through the absorption edge. The Fe L-edge spectra were calibrated against Fe metal powder with the maximum in the first derivative of the $L_3$-edge set to 706.8 eV, and the Mn L-edge spectra were calibrated against Mn metal powder with the maximum in the first derivative of the $L_3$-edge set to 638.7 eV.[19] The spectra were analyzed using the Athena software program.[20]

## ■ RESULTS AND DISCUSSION

**Crystal Structure of the Sample Synthesized in Argon, $Sr_2FeMnO_{5.0}$.** The crystal structure of $Sr_2FeMnO_{5.0}$(Ar) was characterized by X-ray and neutron diffraction. Rietveld refinements were carried out with the GSAS program suite[21] using the EXPGUI interface.[22] The initial refinement was performed on the X-ray data using a $Pm\bar{3}m$ model. The refinement profile is shown in Figure 2a. Although an excellent fit was obtained, the exact Fe and Mn contents, as well as oxygen site occupancy (which, in an ideal case, should be $^5/_6$), remained to be determined by neutron diffraction. For materials containing Fe and Mn, neutron diffraction is an excellent probe because of the large difference between scattering lengths of these elements: 9.45(2) fm for Fe and $-3.75(2)$ fm for Mn. The refined cell parameters and metal atom positions obtained from refinement of the X-ray data were used for refinement of the neutron diffraction data. The results are reported in Tables 2 and 3 and Figure 2b. The oxygen site occupancy from TOF data was refined to 0.833(5), which is exactly the value expected for stoichiometric $Sr_2FeMnO_{5.0}$, indicating the absence of excess oxygen. The refinement with the constant-wavelength neutron diffraction gives a smaller occupation for oxygen. The larger $Q$ range covered by TOF data might be the reason for obtaining a more reasonable O occupancy compared to the constant-wavelength neutron diffraction. Concerning Fe and Mn site occupancies, although the values obtained from TOF and constant-

wavelength neutron data are not the same, they both give values very close to the ideal, that is, within $\sim 4\%$ of 0.50.

Note also the much larger unit cell constant, $a = 3.89328(1)$ Å, compared with the previously reported value, $a = 3.852$ Å, for a sample prepared in air.[15] The Fe(Mn)−O bond length, 1.94539(2) Å, is very close to the average Fe−O and Mn−O distances in $A_2Fe_2O_5$ and $A_2Mn_2O_5$ (A = Ca, Sr), respectively.[1,3,12,13] However, the Sr−O bond in $Sr_2FeMnO_{5.0}$, 2.75120(2) Å, is slightly longer than the average of the lengths observed in $Sr_2Fe_2O_5$ and $Sr_2Mn_2O_5$.[3,13]

Careful inspection of the neutron diffraction data revealed shoulders appearing on almost every major peak, shifted systematically to smaller $d$ spacings; see the inset in Figure 2b. This signaled the presence of a slight amount of another cubic phase with similar composition but smaller cell parameters, which was confirmed by a two-phase Rietveld refinement. The cell parameter for the minority phase is 3.86228(8) Å, as opposed to 3.89328(1) Å for the majority component. The oxygen site occupancy in this second cubic phase was found to be 0.91(3), consistent with $\sim 10\%$ more oxygen compared to the main phase, which is expected, given the smaller cell constant. Although the amount of the second phase was small, the appearance of two phases in the neutron data was puzzling, because there was no indication of a second phase in the high-resolution X-ray data of Figure 2a. As the X-ray data were obtained within a few hours after synthesis whereas the neutron diffraction data were obtained a few weeks later, it was hypothesized that gradual air oxidation of $Sr_2FeMnO_{5.0}$ occurs at room temperature. This was later verified by an X-ray examination of a $Sr_2FeMnO_{5.0}$ sample within 1 h after preparation, as well as a few weeks later. In the next section, we show that a change in the synthesis route such that all of the preparation steps are performed in air (rather than argon) results in a highly oxidized sample with an even smaller cell parameter that still retains the cubic structure. Nevertheless, spontaneous oxidation of $Sr_2FeMnO_{5.0}$ at room temperature is a remarkable phenomenon.

A comparison between the crystal structures of $Sr_2FeMnO_{5.0}$ and our previously studied Ca analogue,[14] $Ca_2FeMnO_5$, is noteworthy. When the two materials are synthesized under argon, the latter crystallizes in the orthorhombic system, space group $Pnma$, with the vacancy-ordered brownmillerite structure. $Mn^{3+}$ preferentially occupies the octahedral sites, with only a few percent of site mixing. A strong octahedral site preference of $Mn^{3+}$ has been demonstrated for $Ca_2GaMnO_5$ and $Sr_2GaMnO_5$ as well.[23−25] Both polyhedra are highly distorted. For the

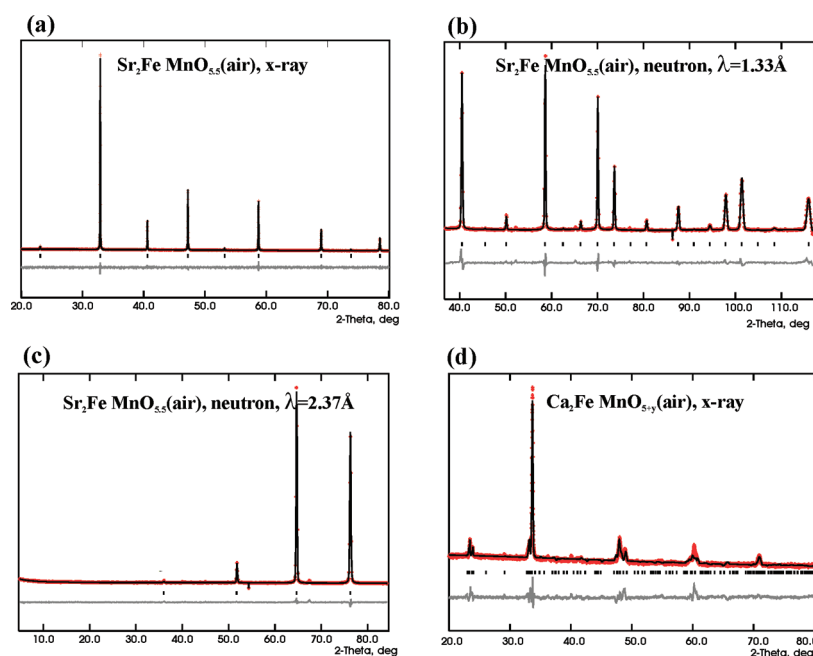**Figure 3.** Rietveld refinement profiles for powder diffraction data. (a-c) Results for $Sr_2FeMnO_{5.5}$(air) ($Pm$-$3m$). X-ray data ($\lambda = 1.54056$ Å) were obtained at 300 K, and neutron data were obtained at 290 K. Panel d shows the powder X-ray profile for $Ca_2FeMnO_{5+y}$(air) and is given for the purpose of comparison, to show that, for the Ca-materials, the synthesis in air results in a brownmillerite structure, similar to the synthesis in Ar.

**Table 4. Refinement Results from Powder X-ray (300 K) and Neutron Diffraction Data (290 K) for $Sr_2FeMnO_{5.5}$ Synthesized in Air**

| space group | $Pm\bar{3}m$ |
|---|---|
| lattice parameters | $a = 3.83075(3)$ Å |
| | $V = 56.215(1)$ Å$^3$ |
| Z | 1 |
| agreement factors | $R_p$ (X-ray, $\lambda = 1.54056$ Å) = 0.0389 |
| | $R_{wp}$ (X-ray, $\lambda =1.54056$ Å) = 0.0510 |
| | $R_p$ (neutron, $\lambda = 1.32858$ Å) = 0.0402 |
| | $R_{wp}$ (neutron, $\lambda = 1.32858$ Å) = 0.0589 |
| | $R_p$ (neutron, $\lambda = 2.36950$ Å) = 0.0235 |
| | $R_{wp}$ (neutron, $\lambda = 2.36950$ Å) = 0.0339 |

| Neutron Results, $\lambda = 1.32858$ Å and $\lambda = 2.36950$ Å, Simultaneous Refinement at 290 K | | | | | |
|---|---|---|---|---|---|
| | x | y | z | occupancy | $U_{iso}$ (Å$^2$) |
| Sr | 0.5 | 0.5 | 0.5 | 1 | 0.0137(9) |
| Fe | 0 | 0 | 0 | 0.482(4) | 0.0030(13) |
| Mn | 0 | 0 | 0 | 0.518(4) | 0.0030(13) |
| O | 0.5 | 0 | 0 | 0.926(10) | 0.0146(5) |



**Figure 4.** $S(Q)$ extended to $Q_{max} = 30$ Å$^{-1}$ at 300 K for $Sr_2FeMnO_{5.0}$ synthesized in argon. The inset shows a strongly modulated background at low $Q$, indicative of short-range ordering of oxygen vacancies. These modulations do not appear in the X-ray data in the same $Q$ range.

octahedra, the four bonds in the $a$−$c$ plane with an average distance of 1.92 Å are significantly shorter than the two bonds out of the plane, 2.22 Å, whereas for the tetrahedra, the four bond lengths range from 1.84 to 1.94 Å. Nonetheless, the average Fe(Mn)−O bond length, 1.97 Å, is similar to that observed in cubic $Sr_2FeMnO_{5.0}$, 1.94539(2) Å.

It is remarkable that substitution of the larger A-site cation, Sr, for Ca destroys the long-range ordering of oxygen vacancies in brownmillerite $Ca_2FeMnO_5$. Note that this does not occur when only Fe or Mn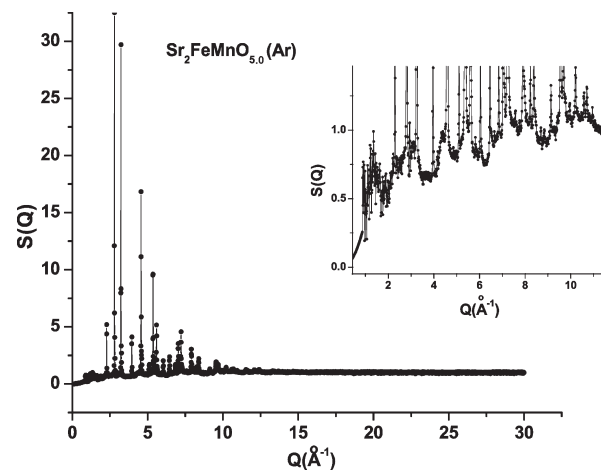 resides on the B/B′ sites, as both $Ca_2Fe_2O_5$ and $Sr_2Fe_2O_5$ are brownmillerites[1−3] and both $Ca_2Mn_2O_5$ and $Sr_2Mn_2O_5$ show the same square-pyramidal geometry for all B/B′ sites.[12,13]

There does not appear to be a simple, straightforward explanation for the remarkable absence of tetrahedral chains in the long-range sense, which is equivalent to the destruction of oxide vacancy order, in proceeding from $Ca_2FeMnO_5$ to $Sr_2FeMnO_5$. As has been noted, vacancy ordering is preserved between $Ca_2Fe_2O_5$ ($Pnma$) and $Sr_2Fe_2O_5$ ($Imma$), albeit in a less ordered manner in the Sr-containing phase.[1−3] Another relevant comparison is between $Ca_2GaMnO_5$ ($I2mb$) and $Sr_2GaMnO_5$

(*Imma*) in which vacancy ordering is retained but attenuated upon substitution of Sr for Ca.[23−25] Only for the B-site combination Fe/Mn does this substitution result in complete destruction of long-range vacancy order. $Ga^{3+}$ and $Fe^{3+}$ are nearly identical in ionic radius, and thus, it is difficult to ascribe an obvious role for the Jahn−Teller ion, $Mn^{3+}$, and its strong octahedral site preference, which has been noted for $Ca_2FeMnO_5$, $Ca_2GaMnO_5$, and $Sr_2GaMnO_5$. $Sr_2FeMnO_5$ was prepared under the same conditions in which the ideal brownmillerite composition is obtained for $Ca_2FeMnO_5$, $Ca_2GaMnO_5$, and $Sr_2GaMnO_5$,[14,25] which is under flowing inert gas, and the oxygen content determined by neutron diffraction from spallation source data is exactly correct. Oxidized phases of $Sr_2Fe_2O_{5+y}$ and $Sr_2GaMnO_{5+y}$ with $y \approx 0.5$ and greater show intermediate structures with well-ordered oxide vacancies,[9,25] which are not observed here. We should note that most of the structural information obtained so far on $Ca_2FeMnO_5$ and $Sr_2FeMnO_5$ is from either neutron or X-ray diffraction and refers to the average structure. Our NPDF and Mössbauer results show that the local structure is more
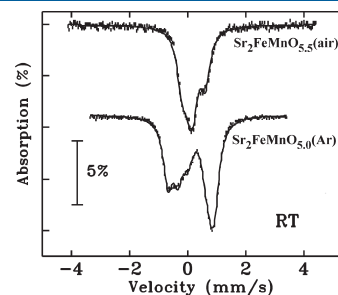


**Figure 6.** Room-temperature Mössbauer spectra for (top) $Sr_2FeMnO_{5.5}$-(air) and (bottom) $Sr_2FeMnO_{5.0}$(Ar). The parameters used to fit the spectra are summarized in Table 5.
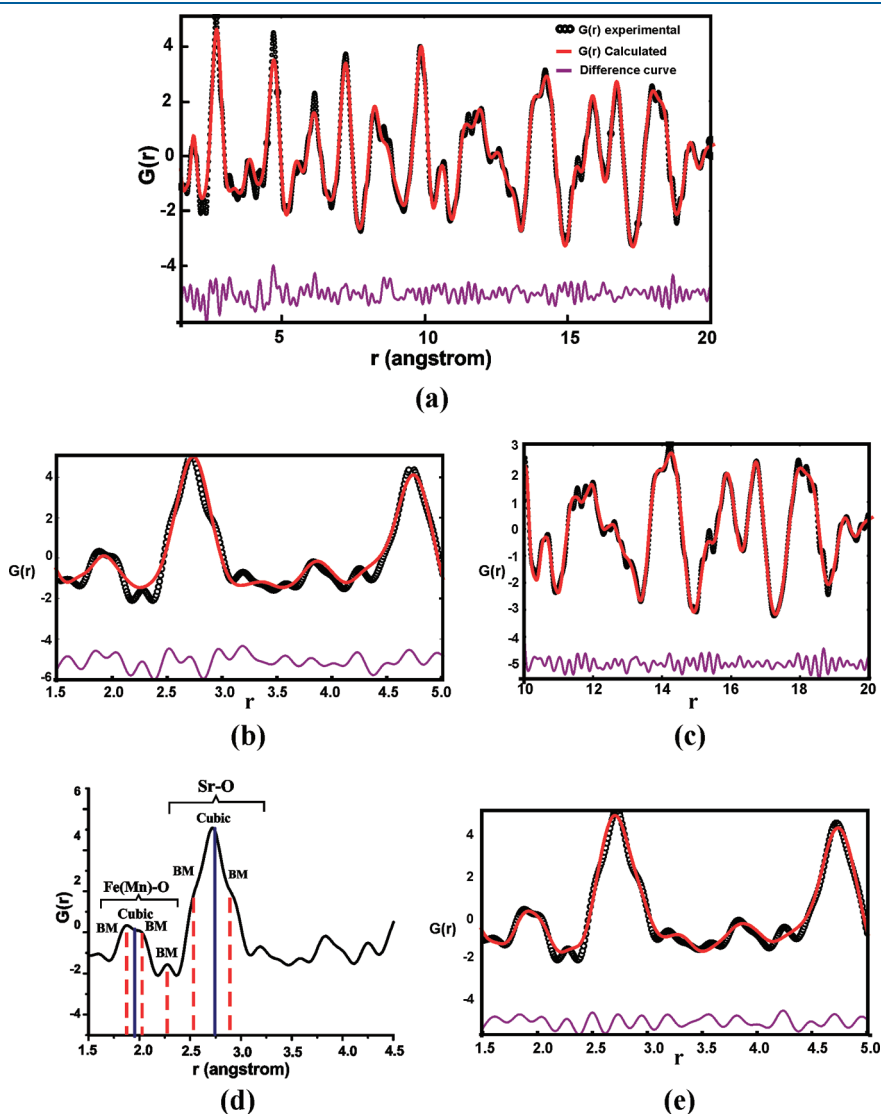


**Figure 5.** (a) $G(r)$ for $Sr_2FeMnO_{5.0}$(Ar), obtained by a Fourier transform of $S(Q)$ truncated at $Q = 30$ Å$^{-1}$. A cubic model, $Pm\overline{3}m$, with disordered oxygen vacancies was used for the fit out to $r = 20$ Å, $R_w = 16.2\%$. (b) $G(r)$ fit with a $Pm\overline{3}m$ model for short $r$, 1.5−5 Å, $R_w = 19.7\%$. (c) $G(r)$ fit with a $Pm\overline{3}m$ model for long $r$, 10−20 Å, $R_w = 12.3\%$. (d) Short-range $G(r)$ compared with interatomic distances corresponding to both a cubic $Pm\overline{3}m$ model (vertical purple lines) and a brownmillerite (BM) $Ibm2$ model (dashed red lines). Note that the features observed in $G(r)$ correspond well to those expected for brownmillerite ordering. (e) $G(r)$ fit with a brownmillerite $Ibm2$ model for short $r$, 1.5−5 Å, $R_w = 13.9\%$.

ordered. In the future, we hope to investigate this material using a more local diffraction probe, namely, electron diffraction (ED). Previous ED studies of apparently ordered BM phases, including $Sr_2Fe_2O_5$, $Ca_2GaMnO_5$, $Sr_2GaMnO_5$, $Ca_2CoAlO_5$, and others, revealed a complex microstructure involving intergrowths of small domains.[2,25,26]

**Crystal Structures of Samples Synthesized in Air.** For the purpose of comparison, both $Ca_2FeMnO_{5+y}$ and $Sr_2FeMnO_{5+y}$ were synthesized.

*Air-Synthesized $Sr_2FeMnO_{5+y}$.* A cubic structure, $Pm\bar{3}m$, was found, as for the argon product, but with a smaller cell parameter, 3.83075(3) Å, which is even smaller than the previously cited

**Table 5. Summary of Fitting Results for Room-Temperature Mössbauer Spectra for $Sr_2FeMnO_{5+y}$**

| | IS (mm/s) | QS (mm/s) | relative area (%) |
|---|---|---|---|
| $Sr_2FeMnO_{5.5}$(air), $y \approx 0.5$ | | | |
| Spectrum fitted using two equal-area doublets, leading to two statistically equivalent models ($\chi^2 = 1.39$) | | | |
| Model 1 | | | |
| site 1 | 0.205(3) | 0.805(6) | |
| site 2 | 0.134(3) | 0.160(8) | |
| Model 2 | | | |
| site 1 | −0.007(3) | 0.411(5) | |
| site 2 | 0.316(3) | 0.554(6) | |
| $Sr_2FeMnO_{5.0}$(Ar), $y \approx 0$ | | | |
| Spectrum best fitted using three quadrupole doublets, a three-site model ($\chi^2 = 1.5$) | | | |
| site 1 | 0.182(3) | 1.60(8) | 41 |
| site 2 | 0.286(4) | 1.15(1) | 34 |
| site 3 | 0.352(5) | 0.67(1) | 25 |

literature value of $a = 3.852$ Å.[15] The refinement profiles for this compound are shown in Figure 3a−c. Unlike the argon product, the material synthesized in air does not show any gradual, spontaneous oxidation in air.

Constant-wavelength neutron diffraction studies indicate an oxygen site occupancy of 0.926(10), which gives $y = 0.56(6)$, consistent with the results of the TGA experiments described in the following section. The Fe and Mn site occupancies were determined to be 0.482(4) and 0.518(4), respectively, close to the ideal value of 0.50. Table 4 summarizes the refinement results for this compound. The Fe(Mn)−O bond length is 1.91981(4) Å, shorter than that observed in the argon material, 1.94539(2) Å, indicating a greater degree of cation oxidation. The contraction of the unit cell also results in shorter Sr−O bonds in the air-synthesized compound, 2.71502(4) Å as opposed to 2.75137(6) Å for the argon material.

*Air-Synthesized $Ca_2FeMnO_{5+y}$.* This material[15] was synthesized for the purpose of comparison. Although there are small differences between our powder pattern and that of ref 15, the occurrence of a brownmillerite phase is clearly evident in both patterns. Figure 3d shows the X-ray refinement profile for this compound in the *Pnma* space group.

Experiments on both Sr and Ca compounds showed that the air oxidation is reversible upon subsequent refiring in argon under the same temperature conditions. The degree of oxidation was determined by thermogravimetric analyses. Based on these measurements, a 1.97% weight loss occurs when a $Ca_2FeMnO_{5+y}$(air) is fired in argon. This corresponds to $y = 0.34$ for the Ca compound. The weight loss for $Sr_2FeMnO_{5+y}$(air) fired in argon is 2.19(6)%, which gives $y = 0.51(1)$.

**Local Structure of Argon-Synthesized $Sr_2FeMnO_{5.0}$.** Although the average structure obtained from refinement of neutron powder diffraction data is clearly cubic, the large atomic displacement parameters indicate that the local structure is likely to be much more complex. To examine the local structure, a neutron pair distribution function analysis was carried out. Figure 4 shows the $S(Q)$ data obtained at 300 K extended to $Q_{max} = 30$ Å$^{-1}$. From the inset, it is clear that the background is highly modulated, indicating considerable short-range order.
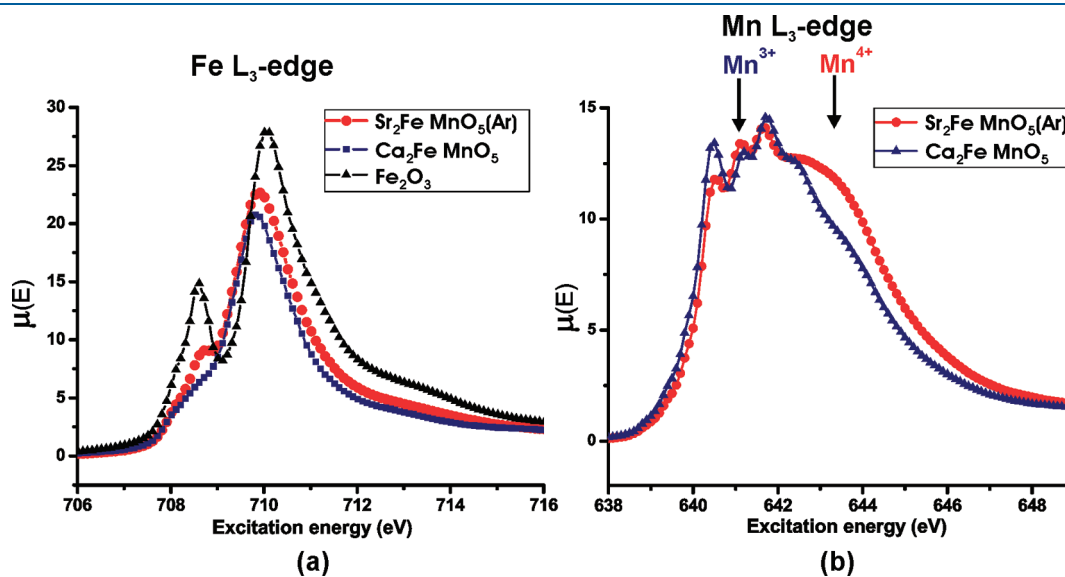


**Figure 7.** XANES spectra for $Sr_2FeMnO_{5.0}$(Ar), compared to those of $Fe_2O_3$ and $Ca_2FeMnO_5$. (a) Fe is in the 3+ state, closely resembling the spectrum for $Ca_2FeMnO_5$. (b) Mn is primarily in the 3+ state. Some $Mn^{4+}$ appears in the spectrum as a result of oxidation of the sample during handling in air.

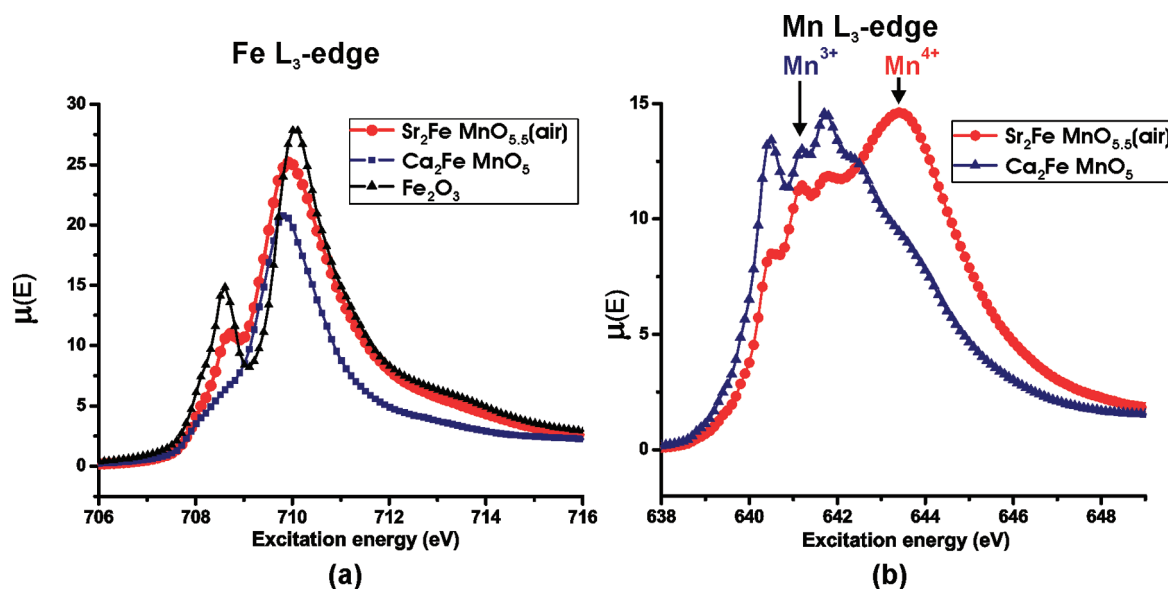7785

dx.doi.org/10.1021/ic200919m |*Inorg. Chem.* 2011, 50, 7779–7791

**Figure 8.** XANES spectra for $Sr_2FeMnO_{5.5}$(air), compared to those of $Fe_2O_3$ and $Ca_2FeMnO_5$. (a) Fe is in the 3+ state, similar to the argon compound. (b) Mn is primarily in the 4+ state, with some $Mn^{3+}$ present.

As these modulations are not seen in the X-ray diffraction data, their origin must be associated with short-range order of oxygen ions. In Figure 5a, the pairwise distribution function, $G(r)$, derived from $S(Q)$ by Fourier transform upon truncation at $Q = 30$ Å$^{-1}$, is shown out to 20 Å. The program PDFGUI[27] was used to perform refinements with the $G(r)$ data to model the local structure.

These data were fit initially with the cubic model, with oxygen vacancy disorder, from 1.5 to 20 Å, as shown, and the agreement is seen to be poor at short $r$. If the fit is done within the ranges of 1.5−5 Å and 10−20 Å separately (Figure 5b,c), the agreement factors, $R_w$, are 19.7% and 12.3%, respectively, emphasizing that the disordered cubic structure is suitable only for the longer distances as the system begins to resemble the average structure. Examination of the short-$r$ data shows the existence of shoulders on many peaks, which are not modeled by the average cubic structure but which correspond to bond distances of a vacancy-ordered brownmillerite structure (Figure 5d). Comparison of the positions of these shoulders with interatomic distances for the brownmillerite $Sr_2Fe_2O_5$[2,3] indicates an excellent match. Note that, for a cubic model, there is only one Fe(Mn)−O distance at ~1.945 Å, whereas a brownmillerite model involves a range of distances from 1.857 to 2.203 Å. Some of these distances are shown in Figure 5d by dashed vertical lines in red. A similar situation applies to the Sr−O distances.

Therefore, a refinement with a brownmillerite model, $Ibm2$, was performed for the data-range from 1.5 to 5 Å (Figure 5e). This model incorporates ordering of oxygen vacancies that results in distinct octahedral (O) and tetrahedral (T) sites. Following the results for $Ca_2FeMnO_5$, a full cation site ordering was assumed with Fe on the T site and Mn on the O site.[14] The refinement results for short $r$ (to $r = 5$ Å) showed a significantly better agreement with the brownmillerite model, $R_w = 13.9\%$, compared to that for the disordered cubic model, $R_w = 19.7\%$. Therefore, the NPDF results suggest that, unlike the average structure, the local structure resembles an oxygen-ordered brownmillerite-type system with Fe mostly in a T site.

**Mössbauer Spectroscopy at Room Temperature.** Mössbauer spectroscopy experiments were performed on both argon-synthesized and air-synthesized samples of $Sr_2FeMnO_{5+y}$, as this technique provides complementary information on the local structure. The results at room temperature are shown in Figure 6 and are summarized in Table 5. In neither case was it possible to find a unique fit. The room-temperature spectrum for $Sr_2FeMnO_{5.0}$(Ar; $y = 0.0$) presents as a severely asymmetric doublet that can be fitted using either three discrete sites or a Gaussian distribution of quadrupole splitting (QS) with strongly correlated isomer shifts (IS) (to reproduce the asymmetry). The latter model yields a relatively poor fit ($\chi^2 \approx 12$) and is unable to fully account for the shape of the low-velocity part of the spectrum in Figure 6. Therefore, the three-site fit, shown as the solid line in Figure 6 and summarized in Table 5, is favored, but caution about the absence of clearly resolved components makes this analysis qualitative in nature. The presence of multiple sites, with different isomer shifts and quadrupole splittings, is qualitatively consistent with the NPDF results, which indicate that the system is not locally cubic. Of the three sites found in the discrete model, all have IS and QS values that are consistent with $Fe^{3+}$ in a site with coordination number less than 6. For comparison, the IS/QS values (in mm/s) for the ordered brownmillerite, $Sr_2Fe_2O_5$, are 0.649/0.411 for the octahedral (O) site and 0.361/0.854 for the tetrahedral site (T).[28] These results are also consistent with general trends shown by a wide range of Fe-based oxides and provide strong evidence that iron is present in the $Fe^{3+}$ state in an environment that is likely tetrahedral.[29] Given the strong O site preference of $Mn^{3+}$ found in $Ca_2FeMnO_5$, $Fe^{3+}$ is expected to be found in T sites in disordered $Sr_2FeMnO_5$.[14]

The room-temperature spectrum of $Sr_2FeMnO_{5.5}$(air; $y = 0.5$) is composed of two overlapping quadrupole doublets with essentially equal areas. This situation inevitably leads to two statistically equivalent models that cannot be distinguished on the basis of $\chi^2$ alone, and the degeneracy can be lifted only by either ruling out one model on the basis of the fitted parameters or preparing a doped sample in which the 1:1 area ratio is changed. The parameters for the two models are given in Table 5.
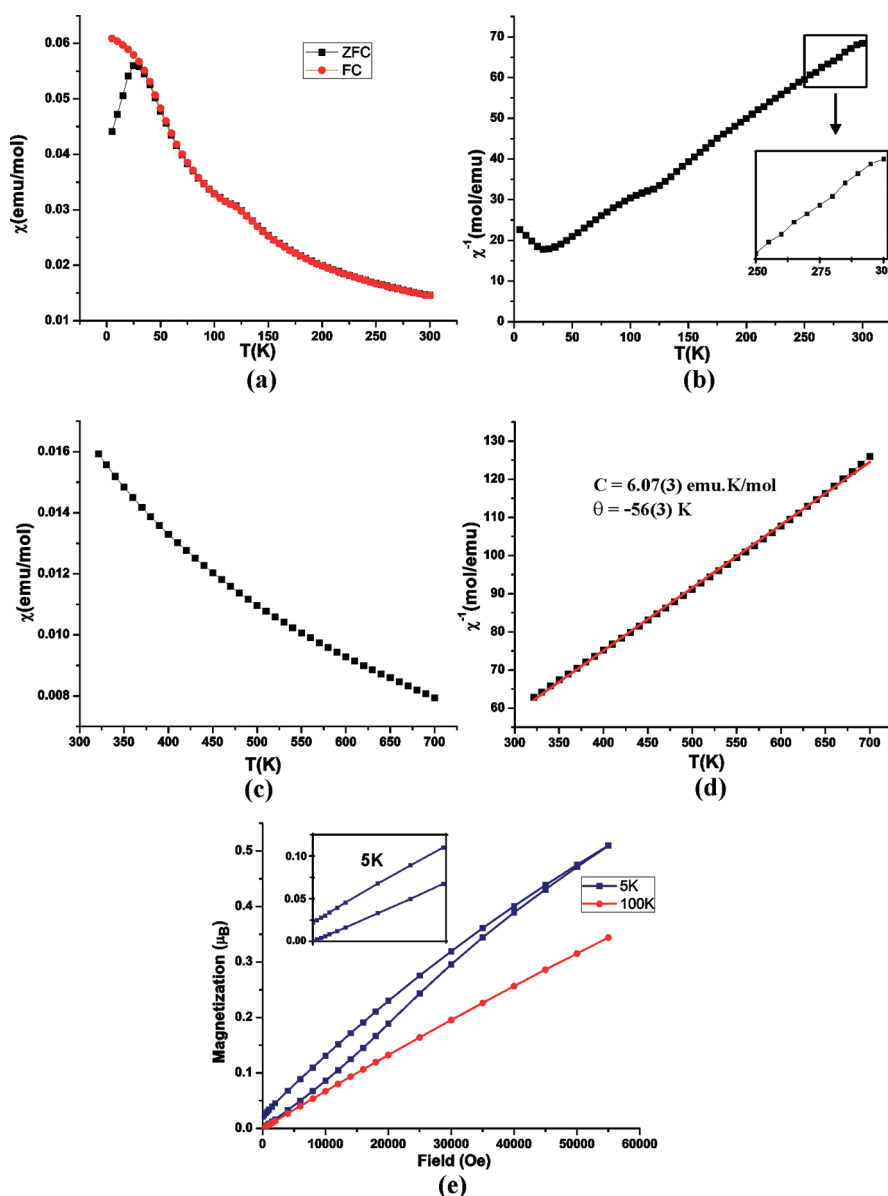
**Figure 9.** (a) ZFC and FC molar susceptibility data for $Sr_2FeMnO_{5.5}$ synthesized in air within the temperature range of 5−300 K. Note the ZFC−FC divergence at ∼25 K. (b) Inverse susceptibility data. The inset shows clearly that a Curie−Weiss regime is not achieved up to 300 K. (c) High-temperature magnetic susceptibility data obtained while heating the sample from 320 to 700 K. (d) Inverse susceptibility data at high temperature fitted to the Curie−Weiss law. The red solid line shows the fit. The Curie constant $C = 6.07(3)$ emu·K/mol is close to the spin-only value for the $Fe^{3+}/Mn^{4+}$ combination (6.25 emu·K/mol), consistent with the XANES results. (e) Isothermal magnetization data at 5 and 100 K. Note the significant hysteresis observed at 5 K, with a remnant magnetization of ∼0.0214 $\mu_B$, magnified in the inset.

The most relevant site-ordered compound for comparison here is $Sr_4Fe_4O_{11}$ with the same oxygen content, which has two Fe sites of equal multiplicity, one square-pyramidal (SP) and one O, with respective IS/QS values of 0.136/0.146 and 0.572/0.434.[29] For both models (Table 5), the fitted parameters, especially the IS values, are inconsistent with O site occupation but support a low-coordination-number environment, possibly SP. The very low IS value of −0.007(3) mm/s found in model 2 might indicate $Fe^{4+}$, but this assignment is not definitive, and it might provide a basis for favoring model 1, as it yields more conventional isomer shifts. The presence of $Fe^{4+}$ can be checked by XANES. In summary, the Mössbauer results support the NPDF analysis in part while indicating a more complex local picture with multiple Fe sites in low-coordination-number environments, T or SP.

**XANES.** To verify the oxidation states and local coordination environments of Fe and Mn, Fe and Mn L-edge X-ray absorption near-edge spectroscopy (XANES) was performed, with $Fe_2O_3$ and $Ca_2FeMnO_5$[14,30] as references. (Note that the cation combination in $Ca_2FeMnO_5$ is $Fe^{3+}/Mn^{3+}$.) These spectra result primarily from a dipolar excitation of 2p electrons to unoccupied 3d states and, as such, provide information on the local coordination environment through examination of the crystal-field-split 3d states.[31] Changes to the screening of the nuclear charge by varying the occupancy of the 3d states lead to shifts in absorption energy, allowing for an examination of metal charge.

For $Sr_2FeMnO_{5.0}(Ar)$, by comparison to $Fe_2O_3$ and $Ca_2FeMnO_5$, the absorption energy of the Fe $L_3$-edge spectrum is consistent with $Fe^{3+}$ (Figure 7a). The spectral line shape shows two peaks,
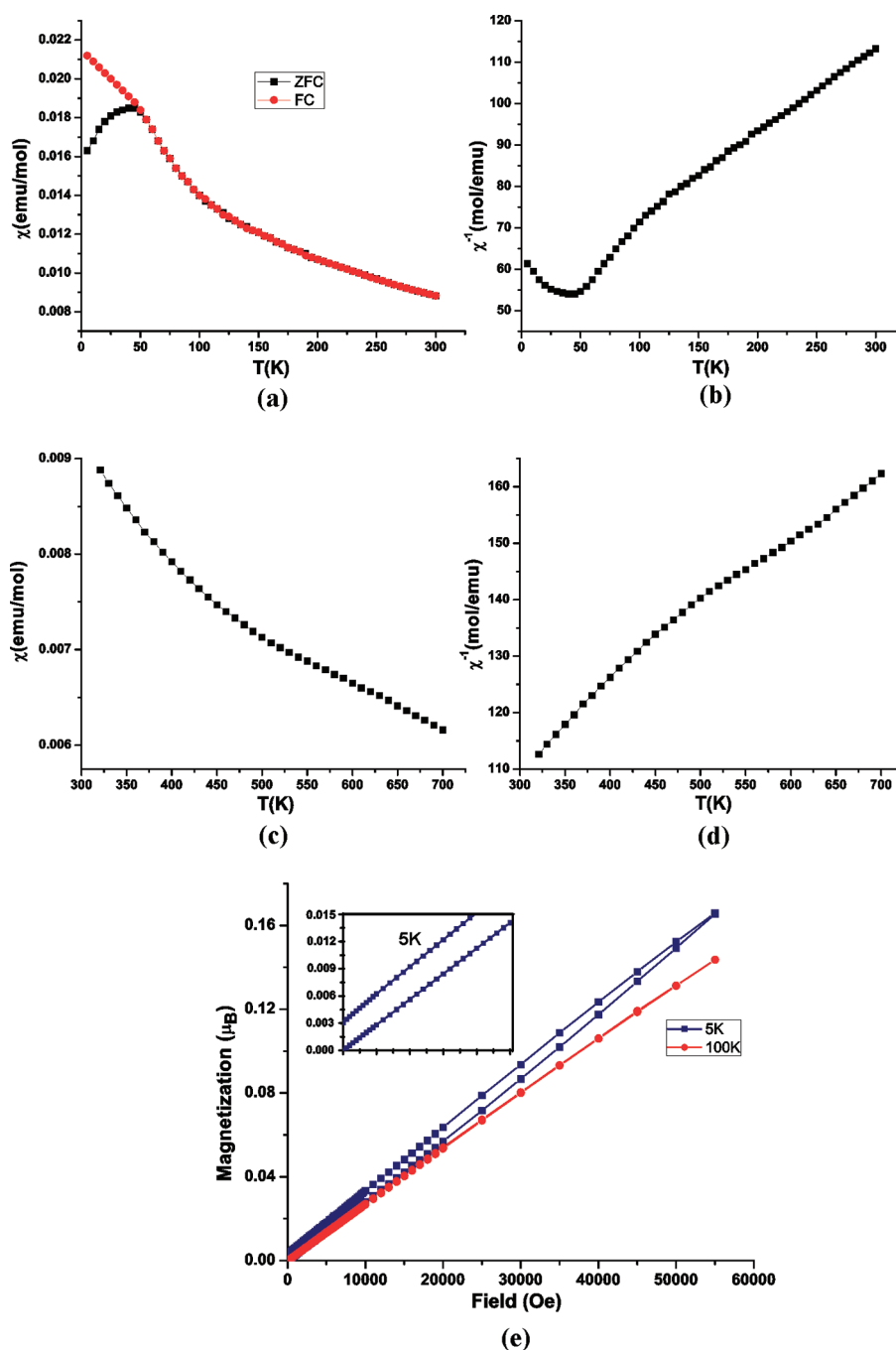
**Figure 10.** (a) ZFC and FC molar susceptibility data for $Sr_2FeMnO_{5.0}$ synthesized in argon within the temperature range of 5–300 K. Note the ZFC–FC divergence at ~50 K. (b) Inverse susceptibility data from 5 to 300 K. (c) Susceptibility data collected while heating the sample from 320 to 700 K. (d) Inverse susceptibility from 320 to 700 K. Note that Curie–Weiss behavior is not seen up to 700 K. (e) Isothermal magnetization data at 5 and 100 K. Note the hysteresis observed at 5 K, with a remnant magnetization of ~0.0031 $\mu_B$, magnified in the inset.

representing crystal-field-split 3d states that are consistent in energy and intensity with Fe atoms primarily occupying a tetrahedral site. The slight increase in intensity of the low-energy peak relative to that from Fe in $Ca_2FeMnO_5$ implies that some Fe atoms in $Sr_2FeMnO_{5.0}$(Ar) might occupy octahedral sites. The corresponding Mn $L_3$-edge spectrum is presented in Figure 7b and indicates that most Mn atoms have a 3+ charge. The high-energy shoulder (see arrow) suggests some presence of $Mn^{4+}$, which was later found to be due to oxidation of the sample during handling.

For $Sr_2FeMnO_{5.5}$(air), the XANES $L_3$-edge data indicate that Fe is in the 3+ state (Figure 8a), which is located mostly in tetrahedral sites but with some occupancy of octahedral sites (i.e., the line shape is between those of $Fe_2O_3$ and $Ca_2FeMnO_5$). There is no indication of $Fe^{4+}$ in these spectra, which is an argument against model 2 for the Mössbauer data. The Mn $L_3$-edge spectrum (Figure 8b) is dominated by $Mn^{4+}$, but some $Mn^{3+}$ is also present.

For both materials, the L-edge data discussed above are consistent with the NPDF and room-temperature Mössbauer studies, which indicated that Fe mostly resides in a tetrahedral site.

7788

dx.doi.org/10.1021/ic200919m |*Inorg. Chem.* 2011, 50, 7779–7791

Comparing spectra for the reduced and oxidized forms, it seems clear that oxidation involves mainly conversion of $Mn^{3+}$ to $Mn^{4+}$ and not $Fe^{3+}$ to $Fe^{4+}$.

**Magnetic Properties.** The magnetic susceptibility data for $Sr_2FeMnO_{5.5}$(air) (Figure 9a) show a zero-field-cooled (ZFC)/field-cooled (FC) data divergence below ~25 K, behavior normally taken as indicative of spin freezing rather than long-range order. The broad maximum observed at ~120 K might indicate short-range magnetic ordering. From the inverse susceptibility data (Figure 9b,c), it is clear that Curie–Weiss behavior is found only above 320 K (Figure 9c). Parameters extracted from a fit between 320 and 700 K (Figure 9d) give a Curie constant of 6.07(3) emu·K/mol, close to the spin-only value for the $Fe^{3+}/Mn^{4+}$ combination (6.25 emu·K/mol), determined by XANES. The magnetization data (Figure 9e) at 5 K show a pronounced hysteresis with a remnant magnetization of ~0.0214 $\mu_B$, indicating the presence of uncompensated moments. These moments are absent at 100 K, where no hysteresis is present in the magnetization data.

The magnetic susceptibility as a function of temperature for $Sr_2FeMnO_{5.0}$(Ar) from 5 to 300 K is shown in Figure 10a. A ZFC/FC divergence similar to the one observed in the air sample is observed but with a much higher apparent $T_f$ value, ~50 K. The 5–300 K inverse susceptibility is plotted in Figure 10b. Even though the plot might appear to reach a linear regime from 250 to 300 K, the high-temperature susceptibility measurements from 300 to 700 K (Figure 10c,d) show that the paramagnetic regime is not achieved even up to 700 K. Isothermal magnetization data (Figure 10e) show a clear hysteresis at 5 K. However, the hysteresis and the remnant magnetization are much smaller than those observed for the air-synthesized compound. Nevertheless, the hysteresis disappears at 100 K, similar to the observation for the air-synthesized material.

The Mössbauer spectra taken at low temperature show magnetic hyperfine splittings for both argon- and air-synthesized materials (Figure 11a–c). For $Sr_2FeMnO_{5.0}$(Ar), the magnetic patterns are broad, largely featureless sextets, indicating that Fe atoms in this system are subject to a very wide range of magnetic environments. The susceptibility anomaly is at about 50 K; however, it is clear from Figure 11a that a magnetic splitting is present for $Sr_2FeMnO_{5.0}$(Ar) at 3 times this temperature. However, closer inspection of the spectra reveals a marked change in appearance below 60 K, as the six hyperfine split lines become distinct. The form of the spectra led to the use of a distribution model to fit them,[17] and the results of this analysis are shown in Figure 11b. The changes upon cooling through $T_f \approx$ 50 K are clear: The average hyperfine field ($\langle B_{hf} \rangle$) increases sharply, and there is a marked drop in the width of the hyperfine field distribution. This likely reflects a change from short-ranged, possibly dynamic, spin correlations above $T_f$ to more organized magnetic ordering below it. The average field of ~50 T at the lowest temperatures is typical of ordered $Fe^{3+}$ compounds. For $Sr_2FeMnO_{5.5}$(air), the spectra presented in Figure 11c show that the magnetic splitting again appears well above the ~25 K event seen in the susceptibility. However, as with the $Sr_2FeMnO_{5.0}$(Ar) sample, there is a marked sharpening of the pattern below the apparent spin-freezing temperature derived from susceptibility. At 4.6 K, the spectrum is both sharper and more complex than that seen for the sample prepared in argon. Although only two equal-area iron sites could be resolved at room temperature, at least four magnetic components are needed to fit the spectrum at 4.6 K. Approximately 50% of the total area is present in two
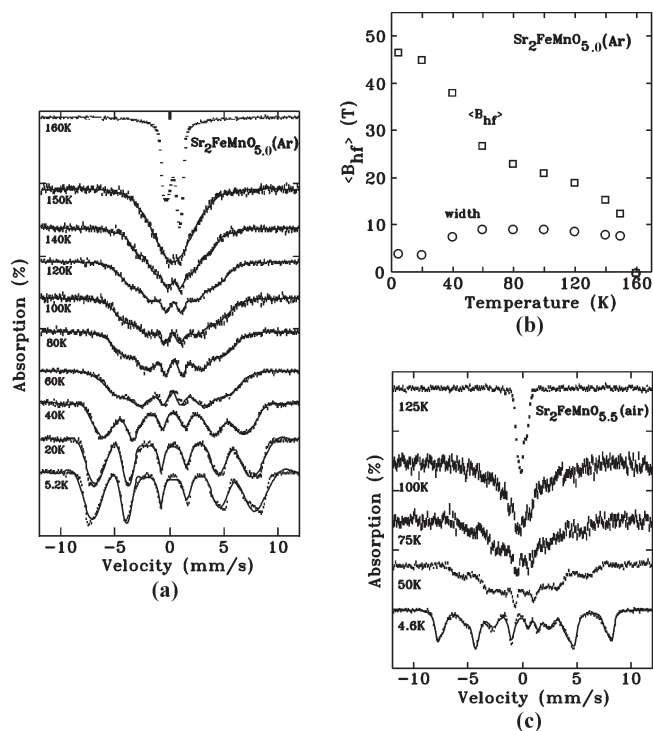


**Figure 11.** (a) Temperature-dependent Mössbauer spectra for $Sr_2FeMnO_{5.0}$ synthesized in argon, with solid lines showing the distribution fits described in the text. (b) Average hyperfine field, $\langle B_{hf} \rangle$, and the width of the distribution derived from the fits for $Sr_2FeMnO_{5.0}$, showing the marked break in behavior below $T \approx 50$ K. (c) Temperature-dependent Mössbauer spectra for $Sr_2FeMnO_{5.5}$ synthesized in air. Note that the short-range magnetic interactions, evident from the hyperfine splittings, persist up to ~150 K for $Sr_2FeMnO_{5.0}$(Ar) and up to ~100 K for $Sr_2FeMnO_{5.5}$(air).
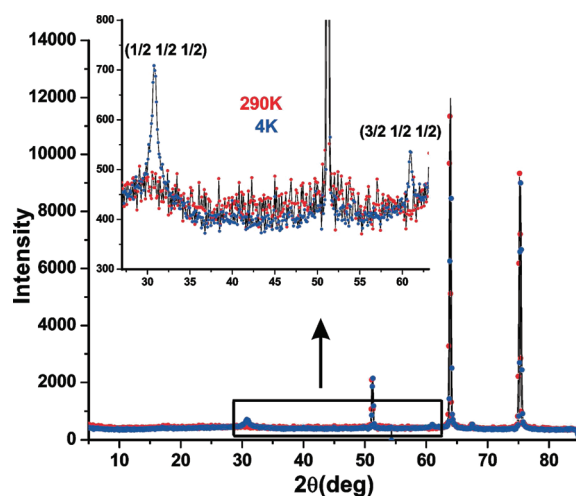


**Figure 12.** Neutron diffraction data for $Sr_2FeMnO_{5.0}$(Ar) at 4 K (blue online) compared with data at 290 K (red online), showing the presence of broad magnetic features at ~31° and 61° that can be indexed as $(^1/_2\ ^1/_2\ ^1/_2)$ and $(^3/_2\ ^1/_2\ ^1/_2)$ on the primitive cubic cell, indicative of short-range G-type magnetic order (inset).

relatively sharp high-field components (50 and 47 T) that can be seen in the form of the two outer lines in Figure 11c. The remaining iron contributes to several much broader components
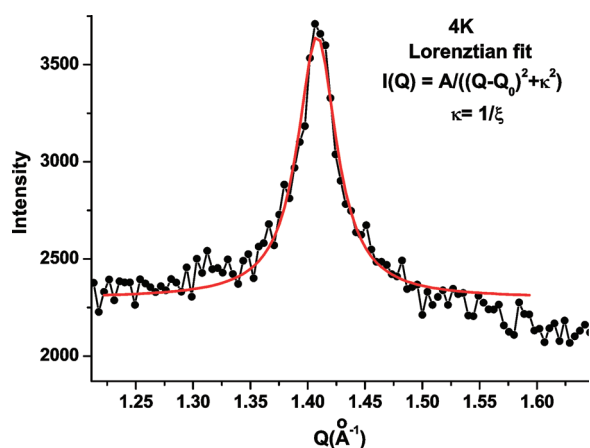
7789

dx.doi.org/10.1021/ic200919m |*Inorg. Chem.* 2011, 50, 7779–7791

**Figure 13.** Fit of the $\left(^1/_2\,{}^1/_2\,{}^1/_2\right)$ magnetic reflection of $Sr_2FeMnO_{5.0}$-(Ar) at 4 K to an Ornstein−Zernike Lorentzian. The fitted values are $Q_0 = 1.408(7)$ Å$^{-1}$ and $\kappa = 0.0207(1)$ Å$^{-1}$. The resulting correlation length is $\xi = 50(1)$ Å after convolution with the resolution function.

with average hyperfine fields ranging from 25 to 30 T. The greatly reduced field and very broad distribution suggests that approximately half of the iron moments in the $Sr_2FeMnO_{5.5}$(air) sample are not fully ordered, even by 5 K, and that they might still be undergoing fluctuations on the Mössbauer time scale ($\sim 10^{-7}$s).

Finally, neutron diffraction data at 4 and 290 K provide more details regarding the low-temperature spin correlations in these materials. In Figure 12, for $Sr_2FeMnO_{5.0}$(Ar), two weak reflections at 30.90° and 60.95° are evident at 4 K, which can be indexed as $\left(^1/_2\,{}^1/_2\,{}^1/_2\right)$ and $\left(^3/_2\,{}^1/_2\,{}^1/_2\right)$ on the chemical cell, respectively, consistent with a G-type magnetic structure. However, the peaks are very weak, broad, and Lorentzian in shape rather than Gaussian, which indicates short-range spin correlations. To estimate the correlation length, the more intense peak at 30.90° ($Q = 1.41$ Å$^{-1}$) was fit to a Lorentzian line shape and analyzed using the Ornstein−Zernike model,[32] $I(Q) = A/[(Q - Q_0)^2 + \kappa^2]$, where $Q = (4\pi \sin \theta)/\lambda$, $A$ is an amplitude, $Q_0$ is the peak center, and $\kappa = 1/\xi$ with $\xi$ being the correlation length (Figure 13). The resulting values are $Q_0 = 1.408(7)$ Å$^{-1}$ and $\xi = 50(1)$ Å, the latter involving a small correction for the resolution function of the diffractometer, indicating that these G-type spin correlations persist to more than 12 unit-cell-axis lengths. Thus, whereas the bulk susceptibility data suggest spin freezing, the actual magnetic ground state appears to consist of short-range domains of local G-type order. This is consistent with the Mössbauer spectra, which show indications below 60 K of a fairly well-ordered state. Very likely, an uncompensated moment is associated with each domain due to either surface spins or perhaps a local spin canting (the local structure is not cubic) giving rise to an unusual type of superparamagnet. Thus, the ZFC/FC divergence in the susceptibility data is understood as a blocking rather than a spin freezing temperature. This proposal is supported by the data of Figure 10e, which show hysteresis below but not above the apparent blocking temperature.

For $Sr_2FeMnO_{5.5}$(air) the results are quite different, as seen in Figure 14. Only one very weak reflection is observed, which can be indexed as $\left(^1/_2\,{}^1/_2\,{}^1/_2\right)$ for a G-type magnetic structure. Surprisingly, this peak is well-fitted by a Gaussian with a width identical within error to the neighboring (100) structure reflection, which indicates that at least some fraction of the sample volume is long-range-ordered. An estimate of the ordered
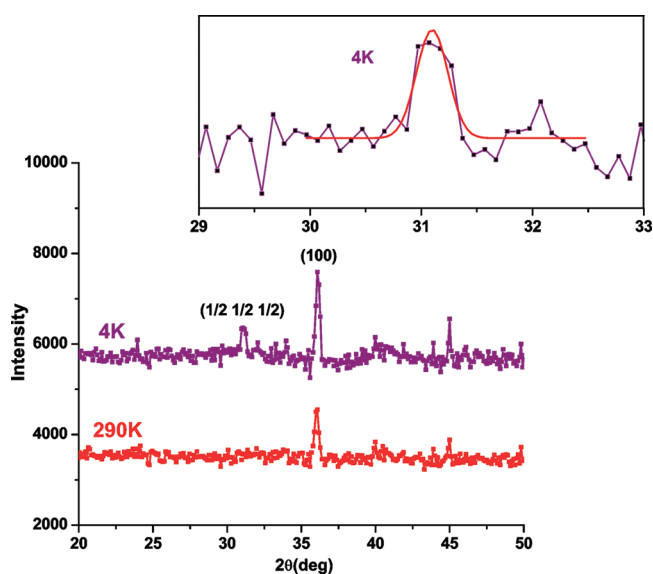


**Figure 14.** Comparison of the low-angle neutron diffraction patterns for $Sr_2FeMnO_{5.5}$(air) at 4 and 290 K showing the development of a $\left(^1/_2\,{}^1/_2\,{}^1/_2\right)$ magnetic peak at 4 K. The inset shows a Gaussian fit of the magnetic peak.

fraction was obtained by comparison of the observed ratio of the $\left(^1/_2\,{}^1/_2\,{}^1/_2\right)/(100)$ reflections with that calculated assuming reasonable ordered moments on Fe and Mn. The result is $\sim 4\%$ volume fraction. This result is also in accord with the Mössbauer observations, which indicated that a large fraction of the Fe moments were not long-range-ordered.

## ■ SUMMARY AND CONCLUSIONS

There is clearly a rather dramatic effect of the A-site cation on both the structure and magnetic properties between $Ca_2FeMnO_{5+y}$ and $Sr_2FeMnO_{5+y}$. For the case of ideal oxygen stoichiometry with both materials prepared in argon, substitution of Sr for Ca induces a change from the vacancy-ordered brownmillerite structure ($Pnma$) to the disordered cubic structure ($Pm\overline{3}m$). Nonetheless, the local structure for $Sr_2FeMnO_{5.0}$ resembles strongly that of a brownmillerite to at least 5 Å. Remarkably, this phase oxidizes spontaneously at room temperature due primarily to the conversion of $Mn^{3+}$ to $Mn^{4+}$.

An equally dramatic effect is seen in the magnetic properties, as brownmillerite $Ca_2FeMnO_5$[14] exhibits long-range antiferromagnetic ordering below $\sim 407$ K with a G-type magnetic structure whereas the cubic perovskite $Sr_2FeMnO_{5.0}$(Ar) shows only a ZFC/FC divergence below $\sim 50$ K in the bulk susceptibility, although Mössbauer spectroscopic data indicate that short-range magnetic correlations persist to much higher temperatures. Neutron diffraction reveals that the magnetic ground state consists at least in part of finite-size domains, $\xi = 50(1)$ Å, with local G-type order. Uncompensated spins associated with these domains give rise to a superparamagnetic behavior. It is remarkable that the effect of the substitution of $Sr^{2+}$ for $Ca^{2+}$ is to destroy the long-range AF G-type order in favor of finite-size domains. $Sr_2FeMnO_{5.5}$(air) behaves differently, showing mainly a very small G-type ordered volume fraction of $\sim 4\%$ at 4 K from neutron data. This is supported by the Mössbauer results that suggest a large fraction of still fluctuating spins at 4 K, indicative of an inhomogeneous magnetic ground state.

## ■ AUTHOR INFORMATION

**Corresponding Author**
*E-mail: greedan@mcmaster.ca.

## ■ REFERENCES

(1) Berggren, J. *Acta Chem. Scand.* **1971**, *25*, 3616.

(2) D'Hondt, H.; Abakumov, A. M.; Hadermann, J.; Kalyuzhnaya, A. S.; Rozova, M. G.; Antipov, E. V.; Tendeloo, G. V. *Chem. Mater.* **2008**, *20*, 7188.

(3) Greaves, C; Jacobson, A. J.; Tofield, B. C.; Fender, B. E. F. *Acta Crystallogr.* **1975**, *B31*, 641.

(4) Schmidt, M.; Campbell, S. J. *J. Solid State Chem.* **2001**, *156*, 292.

(5) Hirone, T. *J. Appl. Phys.* **1965**, *36*, 988.

(6) Takeda, T.; Yamaguchi, Y.; Tomiyoshi, S.; Fukase, M.; Sugimoto, M.; Watanabe, H. *J. Phys. Soc. Jpn.* **1968**, *24*, 446.

(7) Berastegui1, P.; Eriksson, S. G.; Hull, S. *Mater. Res. Bull.* **1999**, *34*, 303.

(8) Schmidt, M.; Campbell, S. J. *J. Phys. Chem. Solids* **2002**, *63*, 2085.

(9) Hodges, J. P.; Short, S.; Jorgensen, J. D.; Xiong, X.; Dabrowski, B.; Mini, S. M.; Kimball, C. W. *J. Solid State Chem.* **2000**, *151*, 190.

(10) Schmidt, M. *J. Phys. Chem. Solids* **2000**, *61*, 1363.

(11) Poeppelmeier., K. R.; Leonowicz, M. E.; Scanlon, J. C.; Longo, J. M.; Yelon, W. B. *J. Solid State Chem.* **1982**, *45*, 71.

(12) Matar, S. F. *Solid State Sci.* **2002**, *4*, 1265.

(13) Suescun, L.; Chmaissem, O.; Mais, J.; Dabrowski, B.; Jorgensen, J. D. *J. Solid State Chem.* **2007**, *180*, 1698.

(14) Ramezanipour, F.; Cowie, B.; Derakhshan, S.; Greedan, J. E.; Cranswick, L. M. D. *J. Solid State Chem.* **2009**, *182*, 153.

(15) Nakahara, Y.; Kato, S.; Sugai, M.; Ohshima, Y.; Makino, K. *Mater. Lett.* **1997**, *30*, 163.

(16) Proffen, T.; Egami, T.; Billinge, S. J. L.; Cheetham, A. K.; Louca, D.; Parise, J. B. *Appl. Phys.* **2002**, *A74*, S163.

(17) Window, B. *J. Phys. E: Sci. Instrum.* **1971**, *4*, 401.

(18) Regier, T.; Krochak, J.; Sham, T. K.; Hu, Y. F.; Thompson, J.; Blyth, R. I. R. *Nucl. Instrum. Methods Phys. Res. A* **2007**, *582*, 93.

(19) Thompson, A.; Attwood, D.; Gullikson, E.; Howells, M.; Kim, K.-J.; Kirz, J.; Kortright, J.; Lindau, I.; Pianetta, P.; Robinson, A.; Scofield, J.; Underwood, J.; Vaughan, D.; Williams, G.; Winick, H. *X-ray Data Booklet*; Lawrence Berkeley National Laboratory: Berkeley, CA, 2009.

(20) Ravel, B.; Newville, M. *J. Synchrotron Radiat.* **2005**, *12*, 537.

(21) Larson A. C.; Von Dreele, R. B. *General Structure Analysis System (GSAS)*; Los Alamos National Laboratory Report LAUR 86-748; Los Alamos National Laboratory: Los Alamos, NM, 1994.

(22) Toby, B. H. *J. Appl. Crystallogr.* **2001**, *34*, 210.

(23) Abakumov, A. M.; Rozova, M. G.; Pavlyuk, B. Ph.; Lobanov, M. V.; Antipov, E. V.; Lebedev, O. I.; Van Tendeloo, G.; Sheptyakov, D. V.; Balagurov, A. M.; Bourée, F. *J. Solid State Chem.* **2001**, *158*, 100.

(24) Wright, A. J.; Palmer, H. M.; Anderson, P. A.; Greaves, C. +*J. Mater. Chem.* **2002**, *12*, 978.

(25) Abakumov, A. M.; Rozova, M. G.; Antipov, E. V. *Russ. Chem. Rev.* **2004**, *73*, 847.

(26) Lambert, S.; Leligny, H.; Grebille, D.; Pelloquin, D.; Raveau, B. *Chem. Mater.* **2002**, *14*, 1818.

(27) Farrow, C. L.; Juhás, P.; Liu, J. W.; Bryndin, D.; Božin, E. S.; Bloch, J.; Proffen, Th.; Billinge, S. J. L. *J. Phys.: Condens. Matter* **2007**, *19*, 335219.

(28) Ravidran, P.; Vidya, R.; Fjellvåg, H.; Kjekshus, A. *Phys. Rev. B* **2008**, *77*, 134448.

(29) Dyar, M. D.; Agresti, D. G.; Schaefer, M. W.; Grant, C. A.; Sklute, E. C. *Annu. Rev. Earth Planet. Sci.* **2006**, *34*, 83.

(30) Grosvenor, A. P.; Greedan, J. E. *J. Phys. Chem. C* **2009**, *113*, 11366.

(31) Grosvenor, A. P.; Ramezanipour, F.; Derakhshan, S.; Maunders, C.; Botton, G. A.; Greedan, J. E. *J. Mater. Chem.* **2009**, *19*, 9213.

(32) Stanley, H. E. *Introduction to Phase Transitions and Critical Phenomena*; Oxford University Press: Oxford, U.K., 1971; p 104.